Supplementary Information

Valorization of agro-industrial fruit peel waste to fluorescent nanocarbon sensor: Ultrasensitive detection of potentially hazardous tropane alkaloid

Athiyanam Venkatesan Ramya* and Manoj Balachandran

Nanocarbon Research Group, Materials Science Research Laboratory, Department of Physics and Electronics, CHRIST (Deemed to be University), Bengaluru - 560029, Karnataka, India

*Corresponding author: Athiyanam Venkatesan Ramya
Tel.: +919880029614
E-mail: avramyaa1@gmail.com

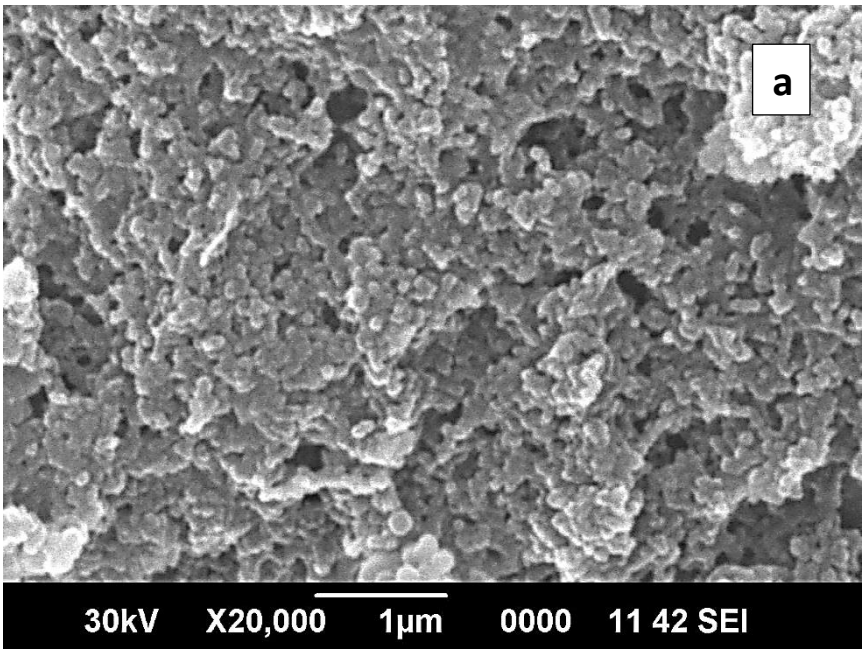

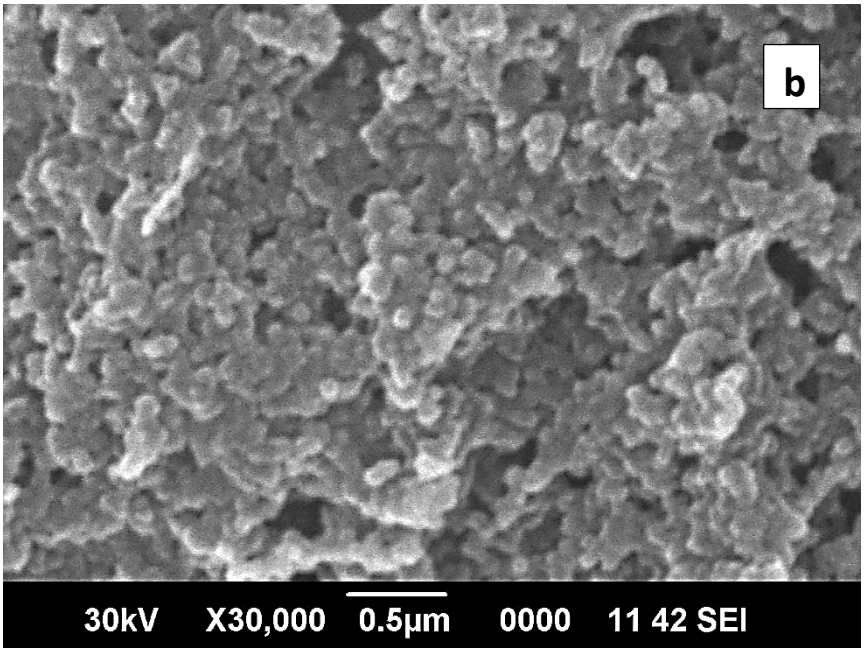

Fig. S1 (a) and (b) SEM images of the synthesized carbon nanostructures showing agglomerated polyhedral morphology

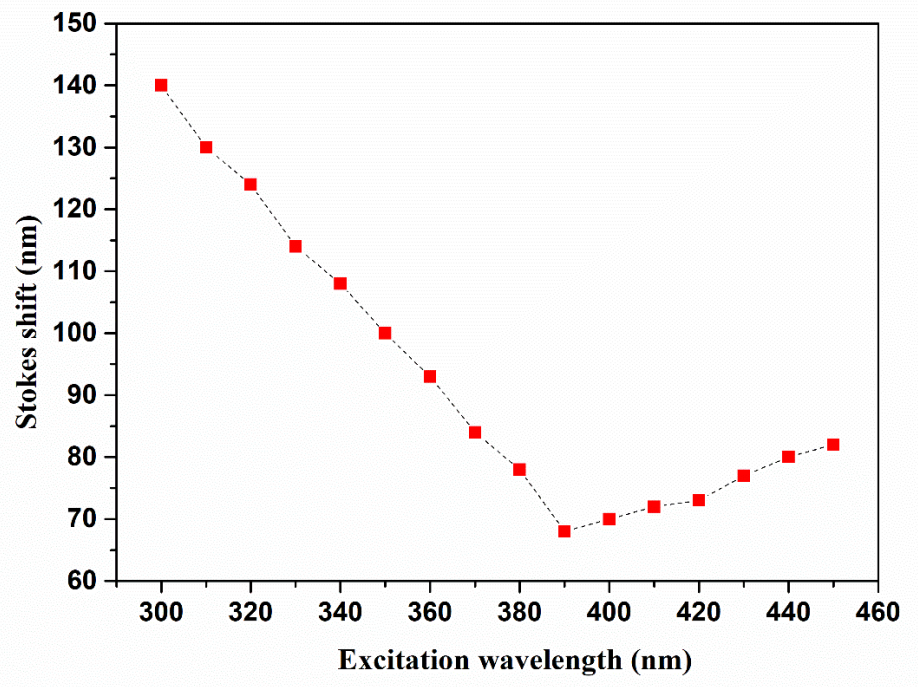

Fig. S2. A plot of the Stokes shift exhibited by fNDC for different excitation wavelengths portraying a nonlinear trend

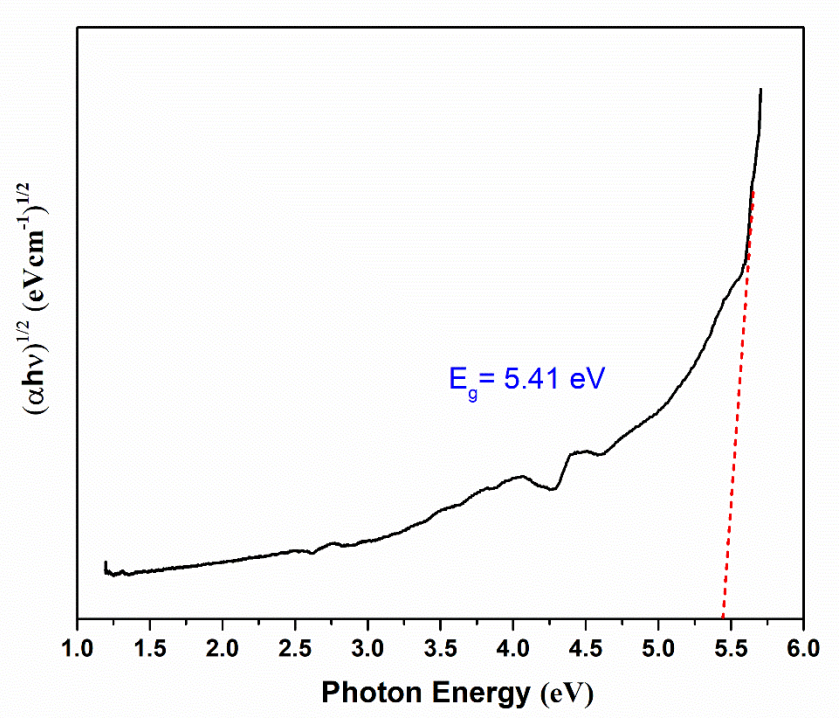

Fig. S3 Tauc plot of the synthesized fNDC exhibiting an optical bandgap of 5.41 eV.

Measurement of fluorescence quantum yield

The quantum yield of fNDC was determined using a standard procedure and quinine sulphate as the standard reference material (Sk and Chattopadhyay, 2014). Absolute values were determined using the following equation:

$$Q_S = Q_R \times \frac{m_S}{m_R} \times \left(\frac{\eta_S}{\eta_R}\right)^2$$

where 'Q_S' and 'Q_R' represent the quantum yield of fNDC and the reference, quinine sulphate. 'm_S' and 'm_R' represent the slope of the integrated fluorescence intensity of fNDC and quinine sulphate, plotted vs. absorbance. 'η_S' and 'η_R'represent the refractive index of the solvents DMF ($\eta_S = 1.43$) and water ($\eta_R = 1.33$). The absorbance of both the reference and the sample was maintained below 0.1 to minimize re-absorption effects. The fluorescence intensity was measured at an excitation wavelength of 360 nm. The values of m_S and m_R were calculated to be 0.69×10^6 and 1.19×10^6, respectively. The quantum yield of fNDC was estimated to be 34.03%.

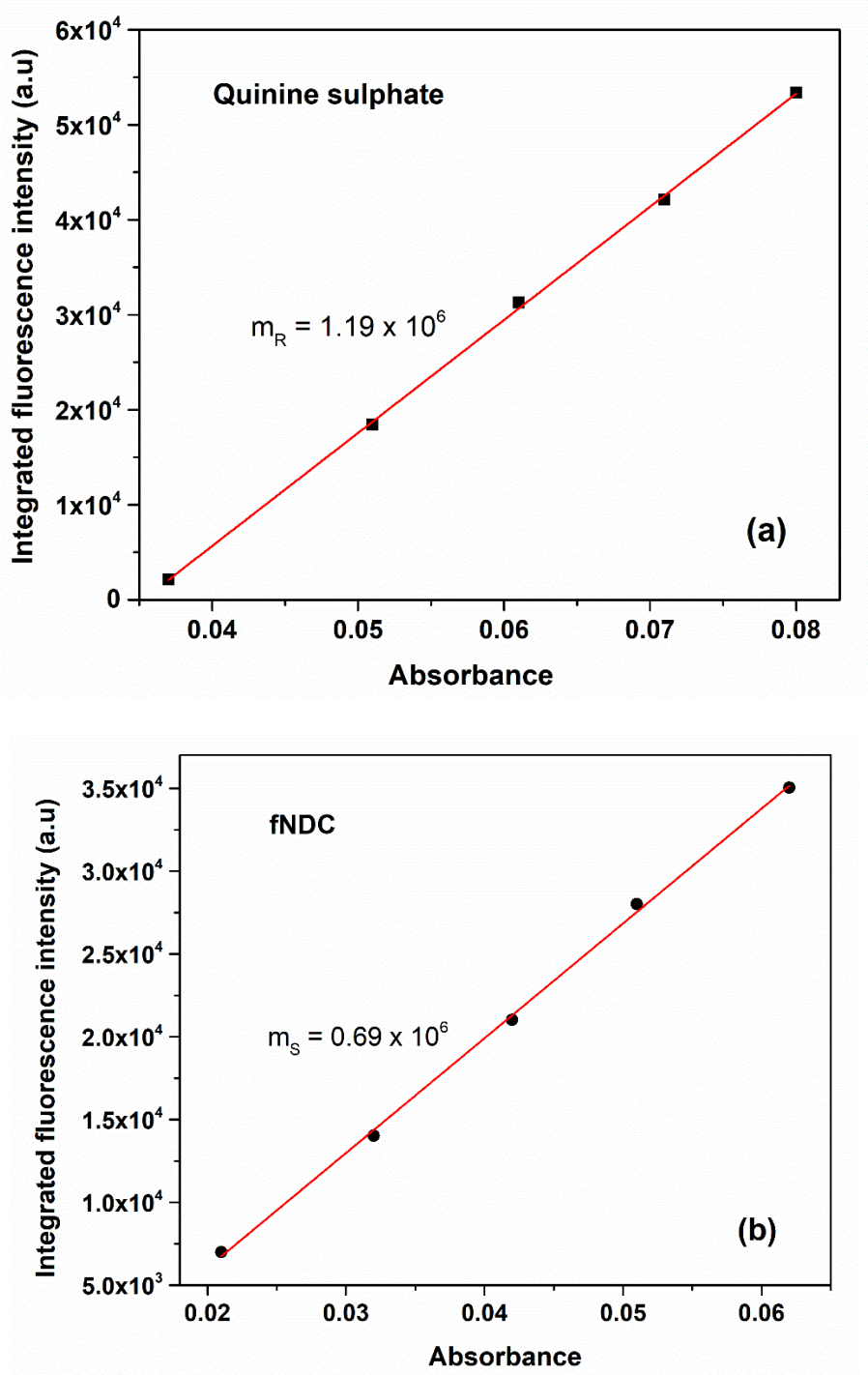

Fig. S4 Plots of integrated fluorescence intensity against absorbance values of (a) Quinine sulphate and (b) fNDC. Red line indicates the data fit.

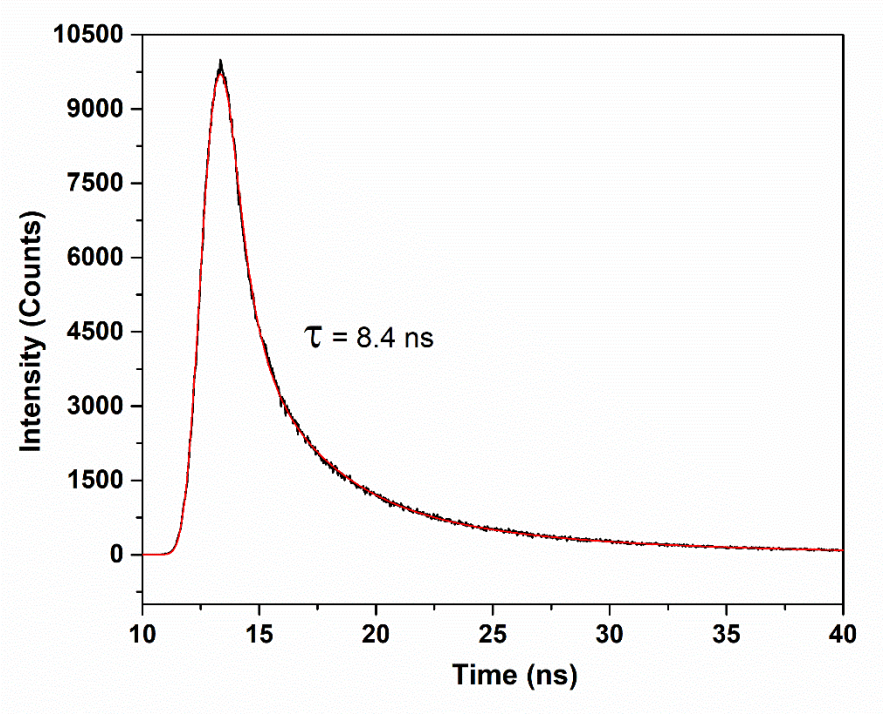

Fig. S5 Fluorescence decay curve of fNDC at 450 nm measured by TCSPC, excited at 340 nm. The black line shows the decay curve, and the red line shows the fitted curve.

Table S1 Fluorescence lifetime measurement of fNDC performed by TCSPC

Sample	**τ_1 (ns)**	**τ_2 (ns)**	**τ_3 (ns)**	**B_1 (%)**	**B_2 (%)**	**B_3 (%)**	**τ (ns)**
fNDC	5.75	0.94	15.58	46.12	17.84	36.04	8.43

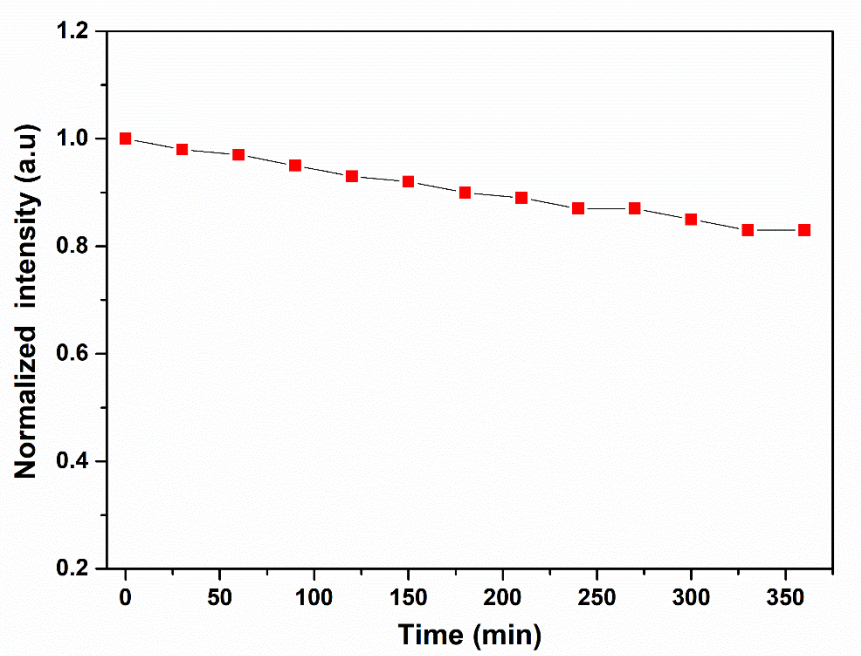

Fig. S6 Photostability of the synthesized fNDC for irradiation up to 6 h

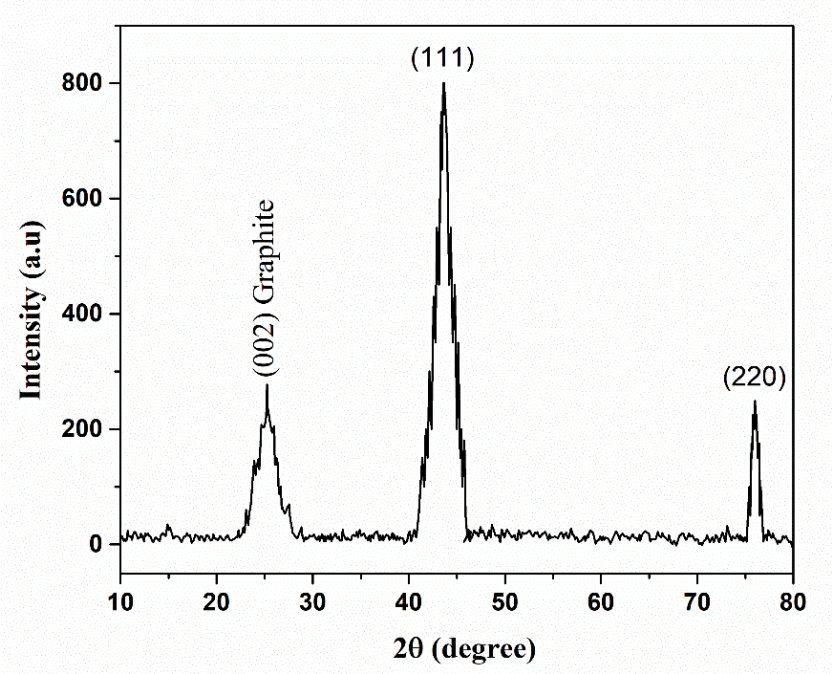

Fig. S7 XRD pattern of the synthesized nanostructure exhibiting the presence of nanodiamond-like carbon phase

Table S2 CHNS elemental analysis of fNDC

C (wt%)	H (wt%)	N (wt%)	S (wt%)	O (wt%) (calculated)
65.86	4.57	0.23	ND	29.34

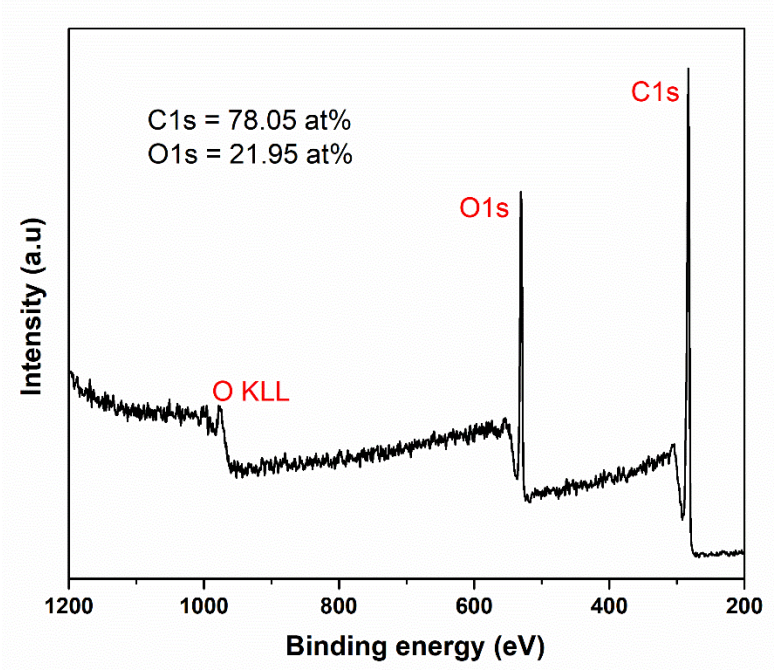

Fig. S8 Survey XPS spectrum of fNDC exhibiting C1s and O1s peaks

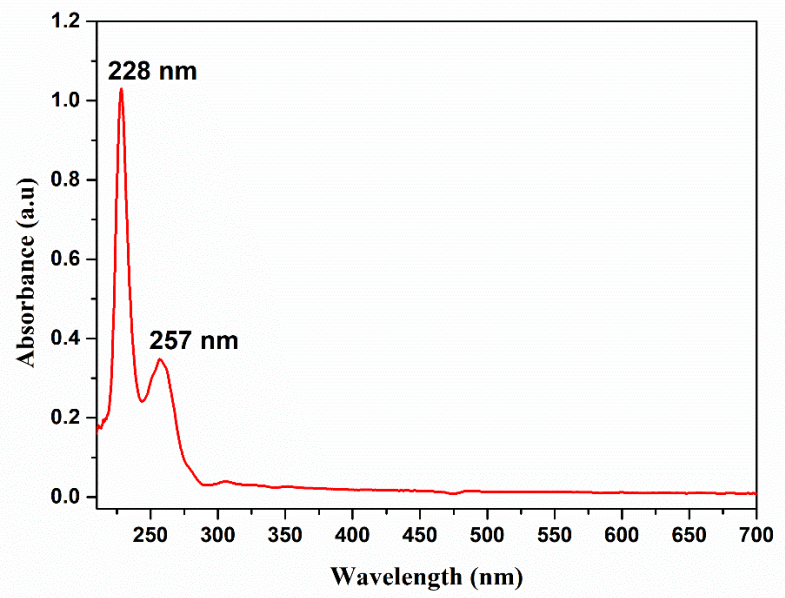

Fig. S9 UV-Visible absorption spectrum of atropine sulphate (AS)

Determination of HOMO and LUMO energy states

The HOMO and LUMO energy levels of fNDC and AS were measured with cyclic voltammetry and UV-Visible spectroscopy. From the CV data, the oxidation potentials (E^{ox}_{onset}) of fNDC and AS were determined to be 1.93 V and 2.16 V (Yen et al., 2019). Their HOMO levels were calculated using the equation:

$$E_{HOMO} = -(4.8 - E_{ox,Fc/Fc+} + E^{ox}_{onset})\ eV$$

where $E_{ox,Fc/Fc+}$ is the oxidation potential of ferrocene/ferrocene^{+} and E^{ox}_{onset} is the onset oxidation potential of the material being tested. Besides, the LUMO energy levels were calculated using the equation:

$$E_{LOMO} = (E_{HOMO} + E_g^{opt})\ eV$$

where E_g^{opt} refers to the optical band gap. The HOMO and LUMO energy levels and the optical band gap values are summarized in Table S3.

Table S3 HOMO and LUMO energy levels and electrochemical energy gap of fNDC and AS calculated from CV

Sample	HOMO (eV)	Energy gap (Optical) (eV)	LUMO (eV)
fNDC	-6.63	5.41	-1.22
AS	-6.86	4.12	-2.74

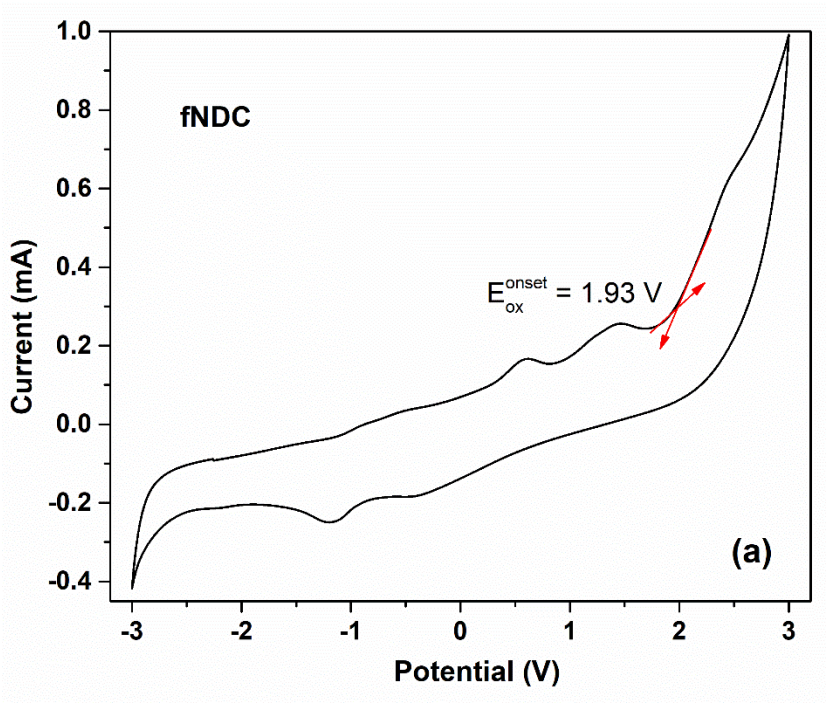

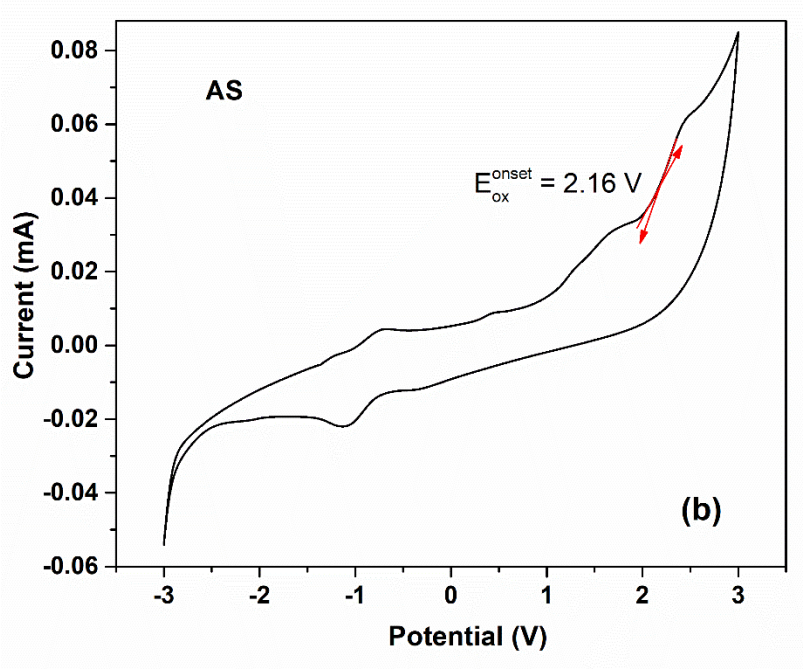

Fig. S10 Cyclic voltammograms of (a) fNDC and (b) AS recorded at a scan rate of 0.5 V/s at ambient condition.

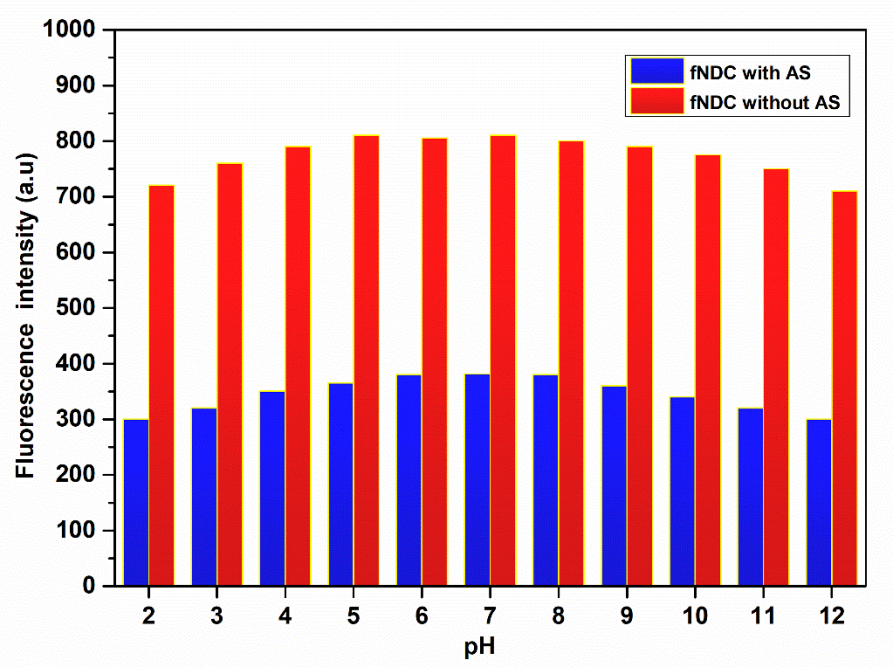

Fig. S11 Fluorescence emission intensity of fNDC with and without atropine sulphate (AS) at different pH conditions

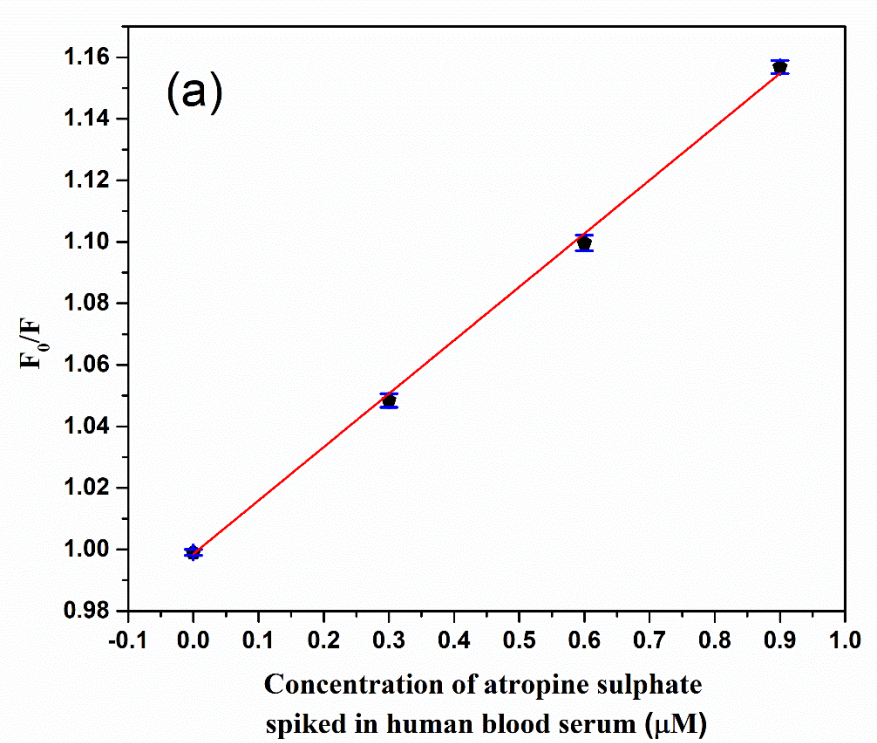

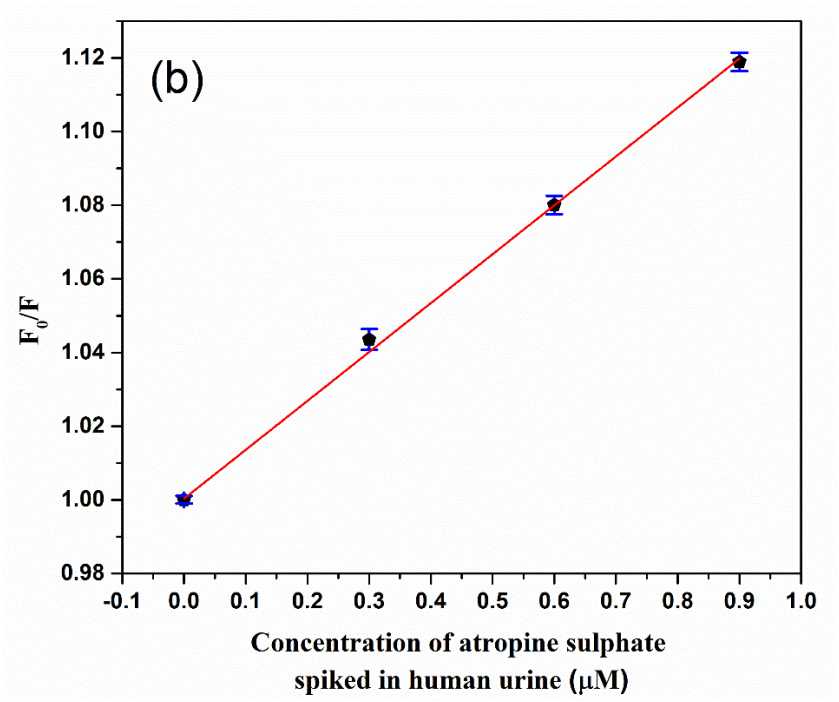
(b)
1.12
1.10
1.08
1.06
1.04
1.02
1.00
0.98
F0/F
-0.1 0.0 0.1 0.2 0.3 0.4 0.5 0.6 0.7 0.8 0.9 1.0
Concentration of atropine sulphate
spiked in human urine (μM)

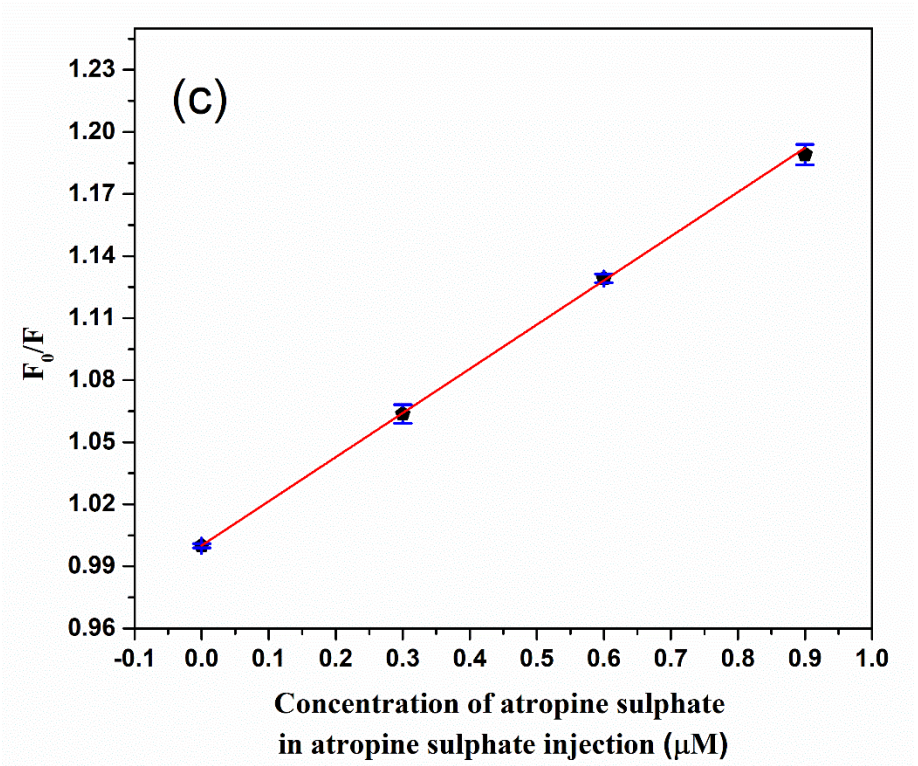
(c)
1.23
1.20
1.17
1.14
1.11
1.08
1.05
1.02
0.99
0.96
F0/F
-0.1 0.0 0.1 0.2 0.3 0.4 0.5 0.6 0.7 0.8 0.9 1.0
Concentration of atropine sulphate
in atropine sulphate injection (μM)

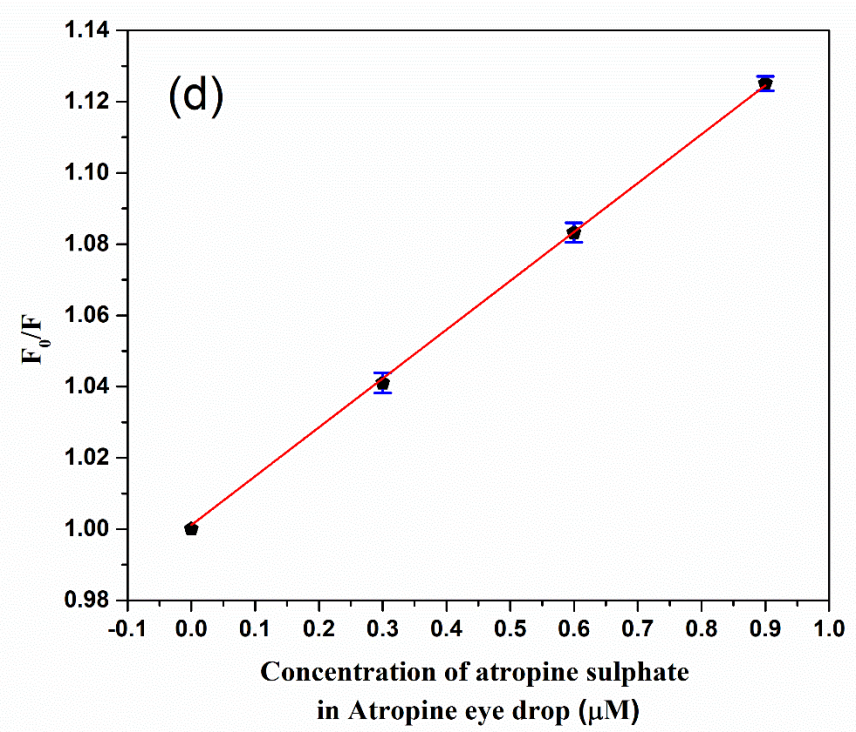

Fig. S12. Determination of atropine sulphate levels in (a) human blood serum and (b) human urine (c) Atropine sulphate injection, and (d) Atropine eye drop

Table S4 A comparison of different sensors for the detection of atropine sulphate

Sensor	Method	Linear Range	LOD	Reference
MIP-GQDs	Fluorimetry	0.5 – 300 ng/mL	0.22 ng/mL	(Khataee et al., 2018)
ds-DNA/PDDA–TiO_2NPs–MWCNTs/PG electrode	Electrochemical	0.6-30 & 30-600 µmol/L	0.03 & 0.10 µmol/L	(Ensafi et al., 2015)
CNTs-Chitosan	Electrochemical	0.1 – 150 µM	16.5 nM	(Mane et al., 2018)
Water - acetonitrile - trifluoracetic acid elution	HPCL	50 – 200 µg/mL	3.75 µg/mL	(Koetz et al., 2017)
DMTD-Ag/CPE	Electrochemical	0.6 – 9 µM	46 nM	(Tiwari et al., 2016)
Mn doped ZnS QDs	Phosphorescence	0 – 9.1 µM	90 nM	(Wu and Fan, 2012)
$[Ru(bpy)^3]^{2+}$/Nafion	Chemiluminescence	0.75 – 100 µM	750 nM	(Brown et al., 2019)
fNDC	Fluorescence	300 nM - 1 µM, and 1 µM -10 µM	34.42 nM, and 356.46 nM	***This Work***

References

Brown, K., McMenemy, M., Palmer, M., Baker, M.J., Robinson, D.W., Allan, P., Dennany, L., 2019. Utilization of an Electrochemiluminescence Sensor for Atropine Determination in Complex Matrices. Anal. Chem. 91, 12369–12376. https://doi.org/10.1021/acs.analchem.9b02905

Ensafi, A.A., Nasr-Esfahani, P., Heydari-Bafrooei, E., Rezaei, B., 2015. Determination of atropine sulfate using a novel sensitive DNA-biosensor based on its interaction on a modified pencil graphite electrode. Talanta 131, 149–155. https://doi.org/10.1016/j.talanta.2014.07.082

Khataee, A., Hassanzadeh, J., Kohan, E., 2018. Specific quantification of atropine using molecularly imprinted polymer on graphene quantum dots. Spectrochim. Acta - Part A Mol. Biomol. Spectrosc. 205, 614–621. https://doi.org/10.1016/j.saa.2018.07.088

Koetz, M., Santos, T.G., Rayane, M., Henriques, A.T., 2017. Quantification of Atropine in Leaves of Atropa Belladonna: Development and Validation of Method By High-Perfomance Liquid Chromatography (Hplc). Drug Anal. Res. 1, 44–49. https://doi.org/10.22456/2527-2616.74150

Mane, S., Narmawala, R., Chatterjee, S., 2018. Selective recognition of atropine in biological fluids and leaves of: Datura stramonium employing a carbon nanotube-chitosan film based biosensor. New J. Chem. 42, 10852–10860. https://doi.org/10.1039/c8nj01312h

Sk, M.P., Chattopadhyay, A., 2014. Induction coil heater prepared highly fluorescent carbon dots as invisible ink and explosive sensor. RSC Adv. 4, 31994–31999. https://doi.org/10.1039/c4ra04264f

Tiwari, M., Kumar, A., Prakash, R., 2016. Nano-porous network of DMTD-Ag coordination polymer for the ultra trace detection of anticholinergic drug. Polymer (Guildf). 82, 66–74. https://doi.org/10.1016/j.polymer.2015.11.017

Wu, H., Fan, Z., 2012. Mn-doped ZnS quantum dots for the room-temperature phosphorescence detection of raceanisodamine hydrochloride and atropine sulfate in biological fluids. Spectrochim. Acta - Part A Mol. Biomol. Spectrosc. 90, 131–134. https://doi.org/10.1016/j.saa.2012.01.041

Yen, Y. Te, Lin, Y.S., Chen, T.Y., Chyueh, S.C., Chang, H.T., 2019. Carbon dots functionalized papers for high-throughput sensing of 4-chloroethcathinone and its analogues in crime sites. R. Soc. Open Sci. 6. https://doi.org/10.1098/rsos.191017